I&EC research
Industrial & Engineering Chemistry Research

Article

Cite This: Ind. Eng. Chem. Res. 2017, 56, 11782-11790

pubs.acs.org/IECR

Increased X-ray Attenuation Efficiency of Graphene-Based Nanocomposite

Juliana Viegas,[†] Liliane A. Silva,[†] Adriana M. S. Batista,[‡] Clascidia A. Furtado,[§] Jefferson P. Nascimento,[§] and Luiz O. Faria*[,§]

[†]Departamento de Engenharia Nuclear, Universidade Federal de Minas Gerais − UFMG, Av. Antônio Carlos, 6627, CEP 31270-970 Belo Horizonte, MG, Brazil

[‡]Departamento de Anatomia e Imagem, Faculdade de Medicina, Universidade Federal de Minas Gerais (UFMG), Av. Prof. Alfredo Balena, 190, CEP 30130-100 Belo Horizonte, MG, Brazil

[§]CDTN-Centro de Desenvolv. da Tecno. Nuclear, Av. Antonio Carlos 6627, CEP 31270-901 Belo Horizonte, MG, Brazil

ABSTRACT: We report an enhanced X-ray shielding effect related to graphene. The mass attenuation coefficients measured for nanocomposites made of poly(vinylidene fluoride) (PVDF) filled with 1.88 wt % functionalized graphene oxides (GO), pyrolytic graphite (PG), multiwalled carbon nanotubes (MWCNT), and amorphous carbon (soot) have been compared. For 6.9 keV photons, the value measured for graphene-based nanocomposite was found to be four times higher than that encountered for the other graphitic-based nanocomposites. The mass attenuation coefficients were measured for X-ray photons with 6.9, 8.1, 17.5, and 22.1 keV, respectively. Fourier transform infrared data revealed that all graphitic composites casted from solution are in the ferroelectric β-phase of PVDF. It is demonstrated that thin films of ferroelectric PVDF/1.88 wt % GO nanocomposite, with thickness of only 0.1 mm, can attenuate 82.9% and 48.5% of X-ray beams with energies of 6.9 and 8.1 keV, respectively. Thus, lightweight, very thin, and lead-free PVDF/GO radiopaque films can be manufactured, offering efficient protection against X-ray radiation for patients and devices in radiology procedures.

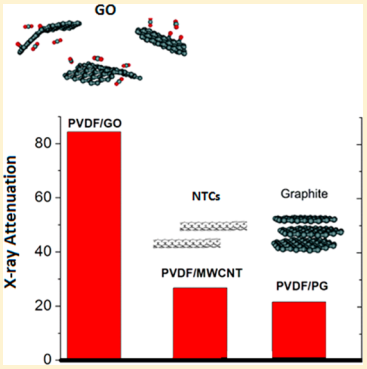

1. INTRODUCTION

In simple terms, graphene is a thin layer of pure carbon; it is a single, tightly packed layer of carbon atoms that are bonded together. It is an allotrope of carbon in the form of a two-dimensional, atomic-scale, hexagonal lattice. Graphene has many unusual properties. It is about 200 times stronger than the strongest steel. It efficiently conducts heat and electricity, is nearly transparent, and shows a large and nonlinear diamagnetism.[1−5] Another notable property of graphene is related to the absorption of electromagnetic radiation: monolayer graphene absorbs ≈2.3% of incident white (visible) light.[6] Graphene also presents some distinctive features for microwave isolation applications.[7] Interestingly, graphene has attracted both academic and industrial interest because it can produce a dramatic improvement in properties of nanocomposites, at very low filler content. The modification of graphene/graphene oxide and the utilization of these materials in the fabrication of nanocomposites with different polymer matrixes have been explored elsewhere.[8]

One of the promising future applications of NTCs or graphene-based nanocomposites is in the field of X-ray attenuation. Interventional radiology procedures such as fluoroscopy provide high doses to skin of patients. Digital mammography and radiography also provide radiation doses to the skin, above the established limits.[9,10] Thus, nowadays, there is great interest in developing new radiation attenuator composites that shield part of the X-ray incident beam, aiming to minimize patient skin injuries. In this context, enhanced X-ray shielding effects of carbon nanotubes (CNTs) have been reported by Fujimori et al., when compared with highly oriented pyrolytic graphite (HOPG). They also demonstrated that CNT-coated fabrics could efficiently absorb 17.5 keV X-ray photons by using polyester fibers coated with only 8 multiwalled carbon nanotubes MWCNTs.[11] It was reported that a textile fabric with thickness of 25 mm attenuated 70% of the X-ray beam. Unexpectedly, the attenuation coefficient of CNTs increased by reducing the sample thickness. This phenomenon cannot be interpreted by the already established X-ray absorption theory. In this context, it is well-known that different nanomaterials have been actively studied using X-ray absorption spectroscopy and that there is an anomaly in X-ray absorption data.[12,13] Additionally, it should be noted that Sawada et al.[14] reported that there is a necessity of carrying out further fundamental studies related to the interaction of X-rays with nanostructured materials.

Encouraged by the above results, the recent discussion about the X-ray absorption features of CNTs and also taking into account that CNTs can be thought of as a graphene sheet (a hexagonal lattice of carbon) rolled into a cylinder, we started a

Received: July 3, 2017
Revised: September 22, 2017
Accepted: September 28, 2017
Published: September 28, 2017

DOI: 10.1021/acs.iecr.7b02711
Ind. Eng. Chem. Res. 2017, 56, 11782−11790

specific investigation about the attenuation coefficients of graphene-based nanocomposites applied to X-ray shielding. We note that graphene-based materials have biomedical applications such as drug/gene delivery, photothermal, photodynamic, and multimodality therapies.[15] Among composites, the polymer-matrix nanocomposites are the most widely studied, with applications in food packaging, medical and optical devices, and microelectronics, among others.[16−18] Poly(vinyl alcohol), poly(methyl methacrylate), and silicones are among the most used polymers in these nanocomposites. In the past two decades, there has been a growing interest in polymer-composite materials for radiation protection, and several studies have reported application of nano- and microcomposite materials to attenuate or absorb high-energy radiation.[11,19,20] Particularly, poly(methyl methacrylate) (PMMA)/MWCNT nanocomposites have been reported to have enhanced shielding attenuation for 105 SEM proton radiation.[21] One of the most radiation-resistant polymer in the market is the poly(vinylidene fluoride) (PVDF) homopolymer. It has attracted interest in the technology and industrial sectors because of its mechanical and ferroelectric properties, its resistance to weathering, and its thermostability. It is a linear semicrystalline homopolymer, and its polymeric chain is composed by the repetition of CH_2-CF_2 monomers. There are five possible distinct crystalline phases, the β-ferroelectric phase being that with many technological applications, finding applications as sensors and transducers.[22] PVDF-based nanocomposites have been highly explored for several applications in order to improve features such as dielectric properties,[23] pressure sensors,[24] electrical conductivity, and dielectric permittivity.[25] The synthesis of PVDF−graphene nanocomposites and their properties have been also explored for applications in several fields.[24,26−28]

Here we report that PVDF/GO nanocomposites, filled with only 1.88 wt % GO, could attenuate X-rays, showing a mass attenuation coefficient similar to the coefficient of aluminum, for photon energies of 6.9, 8.1, 17.5, and 22.1 keV. The mass attenuation coefficients for PVDF-based composites filled with 1.88 wt % pyrolytic graphite, MWCNT, and soot were also investigated for comparison purposes.

2. EXPERIMENTAL SECTION

PVDF was solved in *n*,*n*-dimethylacetamide (DMAc) (0.03 g/mL) with 1 wt % acetic anhydride at 60 °C. Subsequently, the solution was mixed with 1.88% graphitic materials dispersed in solution by sonication. The resulting solution was evaporated. Films of PVDF/graphitic materials with ca. 20 μm were produced. Samples of PVDG/GO filled with 0.5 and 1.0 wt % graphene oxide were also produced.

Concerning the GO production, we have used an improved Hummers's method reported by Marcano et al.[29] The Hummers's method ($KMnO_4$, $NaNO_3$, H_2SO_4) is the most common method used for preparing graphene oxide. However, the improved method used here is done by excluding the $NaNO_3$, increasing the amount of $KMnO_4$, and performing the reaction in a 9:1 mixture of H_2SO_4:H_3PO_4. This improved method provides a greater amount of hydrophilic oxidized graphene material as compared to Hummers's method. Concerning its dispersing state, GO was dispersed in aqueous medium (pH 12, 0.8 mg/mL) by sonication in a Sonics Vibracell VCX 500, with 750 W − 20 kHz, for 30 min.

The dispersion of MWCNTs (5 mg), supplied by Nanocil (NC3100), was done in DMAc (10 mL) and poly(vinylpyrrolidone) [PVP] (5 mg). The dispersion was then mixed with PVDF dissolved in DMAc.

Each film sample was divided into five parts in order to perform the experiments. PVDF homopolymer was supplied by Atochem (France). Graphene oxide (GO) nanosheets were synthesized by the Hummers's method, using graphite supplied by Aldrich as the starting material. Pyrolytic graphite grade-I was supplied by JCM with code number JCM1106.

For photon energies ranging from 6.9 to 22.1 keV, the radiation shielding characterization was performed using an incident monochromatic X-ray beam from the Rigaku diffractometer. In order to generate a monochromatic incident X-ray beam, a nonmonochromatic X-ray was first directed to a single crystal of Si(111). The constructive diffraction from Kα lines of Co (E = 6.9 keV), Cu (E = 8.04), Mo (E = 17.5 keV), and Ag (E = 22.1 keV) X-ray beams were obtained at 2θ approximately equal to 33.13°, 26.60°, 12.96°, and 10.25°, respectively. Different virgin parts of the same film sample were used for irradiation in each photon energy, in order to avoid radio-induced damages by overexposure. For radio-degradation studies, the samples were irradiated with a ^{60}Co source at a constant dose rate (12 kGy/h), with doses up to 1000 kGy.

Composite characterization was performed with Field-emission electron microscopy (FE-SEM), differential scanning calorimetry (DSC), X-ray diffraction (XRD), infrared (FTIR) and ultraviolet−visible (UV−vis) spectroscopy techniques. The FTIR spectra were collected by a Bomem 100 spectrometer in the transmission mode by directly exposing the films to the FTIR beam, for wavenumbers ranging from 200 to 4000 cm^{-1}. The beam was always focused in the center of each ca. 20 μm film sample. UV−vis spectra were taken in a Shimadzu UV-2401 PC spectrometer, for wavelengths ranging from 190 to 900 nm. Thermal behavior studies were made by using a DSC TA Q10, with heating and cooling rates of 10 °C/min, in the second run, from 25 to 200 °C. Typical sample weight ranged from 5 to 10 mg. FE-SEM microscopy was performed on a Sigma VP field emission scanning electron microscope (Zeiss).

3. RESULTS AND DISCUSSION

The mass attenuation coefficient of a volume of a material can be thought of as a variant of absorption cross section, where the effective area is defined per unit mass instead of per particle. The photon mass attenuation coefficients are generally expressed as μ/ρ, where μ is the linear attenuation coefficient (in cm^{-1}) and ρ the material density (in $g{\cdot}cm^{-3}$). They are essential in radiological physics and are dependent upon the absorption and scattering of the incident radiation. Thus, μ/ρ is a function of the photon energy. It is commonly expressed in $cm^2{\cdot}g^{-1}$. The attenuation of an X-ray beam by any material can be written as a function of this coefficient as

$$I = I_0 e^{-(\mu/\rho)\rho x} \quad (1)$$

where I_0 and I are the X-ray intensities of the incident and transmitted beams, respectively, and x is the material thickness. This equation is well-known as the Beer−Lambert law. The term (μ/ρ) has been widely used as an intrinsic value shown in tables containing the X-ray mass attenuation coefficients.[30]

This work aims to investigate the X-ray shielding features of PVDF/GO nanocomposites. We have prepared nanocomposites filled with 0.5, 1.0, and 1.88 wt % graphene oxide. Functionalized graphene was used instead of pure graphene in order to enhance the chances of interaction with the PVDF

DOI: 10.1021/acs.iecr.7b02711
Ind. Eng. Chem. Res. 2017, 56, 11782−11790

main chains, because GO contains COOH and OH bonds mainly linked to the graphene sheet borders. For comparison purposes, we also produced PVDF-based nanocomposites filled with 1.88 wt % other graphitic materials: PVDF/PG, PVDF/MWCNT, and PVDF/soot.

The experimental evaluation of the mass attenuation coefficient for each nanocomposite sample was done by measuring I_0 and I (X-ray intensities of the incident and transmitted beams) following the same setup described by Fujimori et al.[11] and using X-ray tubes made of Co (E = 6.9 keV), Cu (E = 8.04), Mo (E = 17.5 keV), and Ag (E = 22.1 keV). The I_0 and I intensities were obtained at 2θ approximately equal to 33.13°, 26.60°, 12.96°, and 10.25° for each tube, respectively. From eq 1 it is possible to determine the linear attenuation coefficient μ as

$$\mu = -\frac{1}{x}\ln\left(\frac{I}{I_0}\right) \tag{2}$$

The mass attenuation coefficient (μ/ρ) of each nanocomposite is then obtained by dividing μ by its density. The density of a composite made of PVDF filled with graphitic material is calculated in terms of volume fractions as

$$\rho_{comp} = \rho_{PVDF} \cdot w_{PVDF} + \rho_{Graph.Mat.} w_{Graph.Mat.} \tag{3}$$

where w_{PVDF} and $w_{Graph.Mat.}$ are the volume fractions of PVDF and the graphitic material used to fill the nanocomposite, respectively. For nanocomposites filled with 1.88 wt % graphitic material, w_{PVDF} = 0.9812 and $w_{Graph.Mat.}$ = 0.0188.

We started the shielding characterization by irradiating the nanocomposites with 6.9 keV X-ray photons. The results are displayed in Figure 1a,b. Strikingly, a significant X-ray attenuation was observed for the PVDF/GO nanocomposite, when compared to the attenuation observed for nanocomposites filled with pyrolytic graphite, carbon nanotubes, and soot. We remark that the mass attenuation coefficient observed for pure PVDF, i.e. μ/ρ = 19.3 cm^2/g, is in good agreement with the theoretical value (18.4 cm^2/g) calculated by using the NIST photon cross section database. The NIST tool is a web database that can be used to calculate photon cross sections for scattering, photoelectric absorption, and pair production, as well as total attenuation coefficients, for any element, compound, or mixture. The values observed for PVDF/PG and PVDF/soot, 21.4 and 20.5 cm^2/g, respectively, are similar and a little bit higher than that of PVDF. The coefficient observed for the nanocomposite with MWCNT was 26.7 cm^2/g. However, the value observed for PVDF/GO material was much larger than this, i.e. μ/ρ = 84.3 cm^2/g.

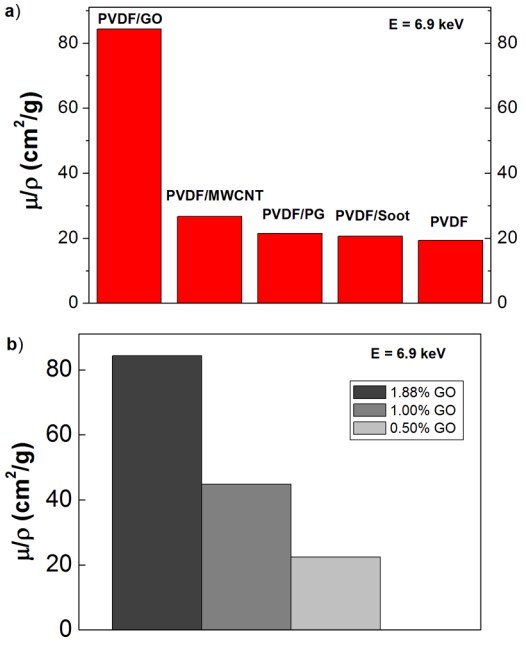

Figure 1. Mass attenuation coefficients of (a) PVDF-based nanocomposites filled with 1.88 wt % graphitic materials (GO, MWCNT, PG, and soot), evaluated for photons with energy of 6.9 keV (Co tube) and (b) of PVDF/GO nanocomposites with different GO concentrations.

In view of the above unexpected mass attenuation coefficient observed for PVDF nanocomposite filled with only 1.88 wt % GO, we extended the experiment for X-ray photon energies beyond 6.9 eV. The idea was to check if the behavior of this attenuation coefficient at different energies was in agreement with the theoretical predicted values. We then irradiated the film samples with X-ray photons with energy of 8.04 keV (Cu tube), 17.5 keV (Mo tube), and 22.1 keV (Ag tube). The observed mass attenuation coefficients are displayed in Figure 2. It is seen in this figure that the observed values for pure

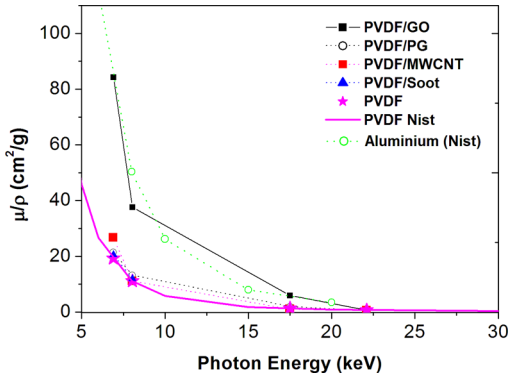

Figure 2. Experimental mass attenuation coefficients of PVDF-based nanocomposites filled with 1.88 wt % graphitic materials (GO, MWCNT, PG, and soot), evaluated for photons with energy of 6.9, 8.04, 17.5, and 22.1 keV.

PVDF and PVDF/PG, PVDF/MWCNT, and PVDF/soot nanocomposites behave as expected. Their mass attenuation coefficients are similar or even a little bit larger than the value for pure PVDF, calculated using the NIST database, for all photon energies studied. There is one exception for E = 6.9 keV, where the value for PVDF/MWCNT is enhanced around 35% when compared to PVDF.

Concerning the above results, an increased value of μ/ρ for a polymer-based nanocomposite filled with MWCNTs was observed by Fujimori et al. They reported that CNT-coated fabrics could efficiently absorb 17.5 keV X-ray photons by using polyester fibers coated with only 8.0 wt % MWCNT and 2.5 wt % ZrO_2.[11] However, as displayed in Figure 2, there is no enhanced value for PVDF/MWCNT at 17.5 keV. That is true only for 6.9 keV photons. In order to explain this apparent divergence, we remark that our composite is filled with only 1.88 wt % MWCNT, without ZrO_2 particles. Additionally, the geometry of the NTCs distribution inside the polymer matrix is different because they used polyester filaments coated with

DOI: 10.1021/acs.iecr.7b02711
Ind. Eng. Chem. Res. 2017, 56, 11782−11790

MWCNT, and in this work, we mixed solved PVDF with NTCs dispersed in solution.

We may now discuss the anomaly in the mass attenuation coefficients observed for PVDF/GO nanocomposites. For comparison purposes we also plotted in Figure 2 the theoretical values for aluminum published in the NIST database. Both PVDF/GO and aluminum have similar attenuation coefficients in the energy interval studied. As can be seen in Figure 2, the PVDF/GO attenuation coefficients start to become larger than those coefficients observed for pure PVDF, and also for the nanocomposites filled with MWCNT, PG, and soot, for photon energies below ∼22 keV. We note that, according to the simulation performed using the NIST database in order to calculate the GO and PVDF attenuation coefficients shown in Figure 3, this is around the energy value where the

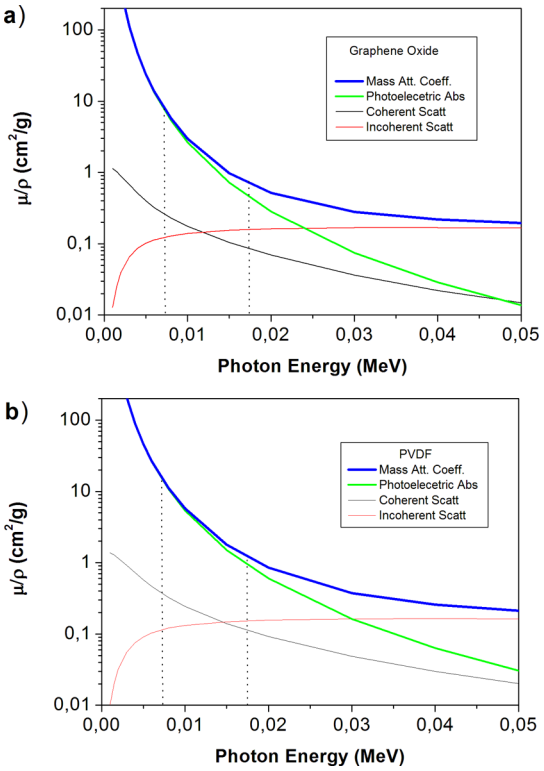

Figure 3. Mass attenuation coefficients calculated using NIST database for (a) graphene oxide and (b) PVDF. The dotted lines delimit the energy range where the experimental values of μ/ρ for PVDF/GO are larger than those measured for PVDF/MWCNT, PVDF/PG, and PVDF/soot, i.e., from 6.9 to 17.5 keV.

photoelectric absorption starts to predominate against coherent and incoherent scattering, toward lower energies. Recall that one of the notable properties of graphene is related to the absorption of electromagnetic radiation. Nair et al.[6] reported that one monolayer of graphene absorbs ≈2.3% of incident white (visible) light, and also, as reported by Rubrice et al.,[7] it presents some distinctive features for microwave isolation applications.[7] Thus, we see now that graphene also has a distinctive property to absorb electromagnetic radiation, with higher mass attenuation coefficient than predicted by the theoretical models, for X-rays photons with energies below 22 keV.

As reported by Fugimore et al.,[11] cylindrically rolled graphene structures (nanotubes) revealed an increased attenuation coefficient for decreasing sample thickness, when exposed to 17.5 keV X-ray photons. According to the authors, this phenomenon does not follow any conventional rule stating that the mass attenuation coefficients are inherent to the type of elements contained within the material. In the same experiment, graphene oxide exhibiting a flat sheet structure did not show any significant dependence of mass attenuation coefficient with respect to thickness. In our work, we have detected an anomaly in the mass attenuation coefficients observed for PVDF/GO nanocomposites: the addition of 1.88% graphene oxide in a PVDF matrix resulted in an increased X-ray attenuation, when compared to the attenuation of PVDF alone, for X-ray photons with energies ranging from 6.9 to 17.5 keV. However, PVDF nanocomposites filled with 1.88% MWCNT did not show any relevant change in the X-ray attenuation, except for a small increase when exposed to photons with energy of 6.9 keV. In order to explain these conflicting results, we note that, in our experiment, the graphene oxide and MWCNT were dispersed into a polymeric matrix, differently from the Fujimori experiment where the X-ray attenuations were measured for pure samples.

In this context, Bludov et al.[31] performed a theoretical work and reported an unusual reflection of electromagnetic radiation from a stack of graphene layers at oblique incidence. The interaction of electromagnetic (EM) radiation with single-layer graphene and a stack of parallel graphene sheets at arbitrary angles of incidence was found to behavior qualitatively differently for transverse magnetic (or p-polarized) and transverse electric (or s-polarized) waves. In particular, the absorbance of single-layer graphene attains minimum (maximum) for p (s) polarization, at the angle of total internal reflection when the electromagnetic radiation comes from a medium with a higher dielectric constant. In the case of equal dielectric constants of the media above and beneath graphene, for grazing incidence, graphene is almost 100% transparent to p-polarized waves. We remark that in our experiment, the graphene sheets (ε = ∼3.0) are imbedded in a dielectric medium with higher dielectric constant, the PVDF homopolymer (ε = ∼9.5), opening a possible way to explain the increased X-ray attenuation of PVDF/OG nanocomposites. However, Bludov et al. also reported that the results were simulated to EM fields just for energies in the terahertz to far-infrared (FIR) range, which is far below the energy range used in our work.

Another possible and more plausible explanation comes from an interesting anomalous behavior observed for graphene sheets related to the thermal expansion coefficient (TEC). We remark that the linear attenuation coefficient (μ) is dependent on the number of atoms inside a fixed volume. For instances, a cube of ice has an attenuation coefficient higher than the water vapor, because in the same volume of vapor there will be a smaller number of atoms. In this sense, μ is dependent on TEC for all materials. In nature, the TEC for known materials increases for increasing temperatures, and consequently, the linear attenuation coefficient, which is expressed as $I = I_0 e^{-\mu x}$ (eq 1), decreases as the temperature is increased. Recently, Yoon et al.[32] estimated the temperature dependence of the TEC of single-layered graphene with temperature-dependent Raman spectroscopy in the temperature range between 200 and 400 K. It was found to be negative in the whole range, which is in contradiction to a previous estimate, and it varies strongly with temperature with a room-temperature value of $(-8.0 \pm 0.7) \times 10^{-6}$ K^{-1}. At 400 K, the TEC decreases to -40×10^{-6}

DOI: 10.1021/acs.iecr.7b02711
Ind. Eng. Chem. Res. 2017, 56, 11782−11790

K^{-1}. This means that the graphene lattice retracts when the temperature arises, diminishing the number of atoms inside a virtual volume, in the same way that it happens when ice is turned to water vapor. In other words, the linear attenuation coefficient of graphene sheets will increase for increasing temperatures above room temperature. The above observations lead us to consider the behavior of the graphene sheet temperature when it is exposed to X-rays. We remark that the two-dimensional carbon material graphene possesses a number of unique and extraordinary properties, such as high charge carrier mobility, an electronic energy spectrum without a gap between the conduction and valence bands, and frequency-independent absorption of EM radiation. When a material is exposed to X-ray radiation, electron−hole pairs are produced and their motion generates the photothermal effect. When electrons move through a metal, they carry electric charge and energy. The former is responsible for the electric current, the latter for the heat current. In graphene sheets, a photon absorption excites an e−h pair that leads to the ultrafast heating of the lattice, due to its high charge carrier mobility. Assuming that the TEC of graphene is negative, different from other materials including carbon nanotubes where TEC is positive, the ultrafast heating would then increase the linear attenuation coefficient during the X-ray irradiation.

The investigation about the distribution of the different graphitic materials into the PVDF polymeric matrix and their influence in the PVDF crystalline structure and chain conformation was done performing SEM micrographs, FTIR spectrometry, and DSC scans.

SEM micrographs of pure PVDF and PVDF nanocomposites filled with 1.88 wt % GO, MWCNT, PG, and soot are shown in Figure 4. The spherical surfaces seen in the PVDF micrograph

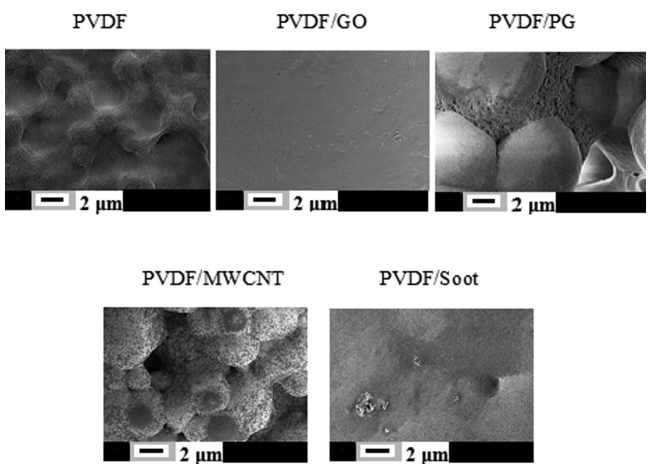

Figure 4. SEM micrographs of PVDF homopolymer filled with 1.88 wt % GO, PG, MWCNT, and soot. The scale bar is 2 μm.

are spherical aggregates of lamellar crystallites, called "spherulites". We remark that spherulite is a big crystalline structure when compared to a crystalline lamella. In fact, spherulites are made of radial fibers that grow radially outward from the crystalline nuclei in the melt upon cooling or recrystallization from casting. These fibers are in reality stacks of very thin platelet-like crystals called lamellae, which are ∼10 nm thick and several micrometers in lateral extension. It is interesting to observe that among all nanocomposites, the spherulites are not seen in the PVDF/GO nanocomposite. Thus, we may say that there is a different interaction among the functionalized GO nanosheets and PVDF chains that prevents the formation of big crystalline structures. On the other hand, the micrograph of PVDF/PG nanocomposite shows clearly the nanosheets accommodated between adjacent spherulite surfaces, as shown in Figures 4 and 5. In this case, the presence of pyrolytic graphite seems to provide special conditions that allow the formation of bigger spherulites.

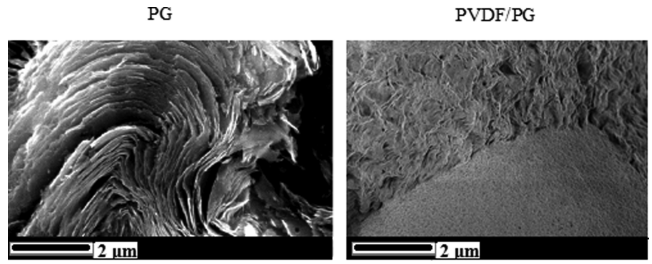

Figure 5. Pure pyrolytic graphite (left) and PVDF/PG nanocomposite (right) micrographs, showing how the PG is accommodated between adjacent spherulite surfaces.

To check why spherulites are not seen in the PVDF/GO nanocomposite, SEM micrographs of pure PVDF and PVDF/GO nanocomposites filled with 0.5, 1.0, and 1.88 wt % graphene oxide are shown in Figure 6 (upper and midle). It becomes clear that, for lower amounts of GO, 0.5 and 1.0 wt %, the spherulites are still formed. Thus, it seems that amount of GO in the PVDF matrix has fundamental influence in the formation of larger crystalline structures. On the other hand, it

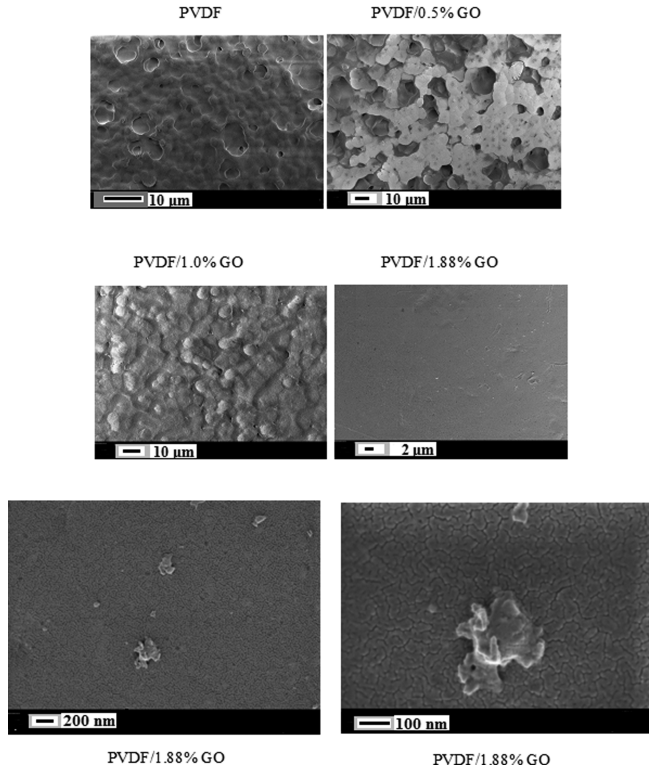

Figure 6. SEM micrographs of PVDF pristine and filled with 0.5%, 1.0%, and 1.88% GO (upper). Two magnified micrographs for PVDF/GO filled with 1.88% (bottom) showing four large GO layered aggregates and several small ones dispersed on the surface (left) and a zoomed-in view of the larger layered aggregate (right).

DOI: 10.1021/acs.iecr.7b02711
Ind. Eng. Chem. Res. 2017, 56, 11782−11790

has been reported that the size of solution crystallized spherulites of PVDF depends on initial polymer concentration,[33] temperature,[34] and also on the substrate used.[35] However, it is interesting to observe that among these three parameters, only one refers to the mixing of PVDF with another material, in this case the initial polymer concentration. In fact, Ma et al. reported that when PVDF (w = 0.7) is mixed with poly(methyl methacrylate) (PMMA) (w = 0.3), the size of spherulites decreases for increased initial concentration.[33] We remark that, in our experiment, the parameters temperature and substrate were the same for all samples produced. Thus, it seems that the changes in the initial polymer concentration caused by the addition of GO could be linked to the lack of spherulites for GO amounts higher than 1 wt %. Also in Figure 6 (bottom) two magnified SEM micrographs of PVDF/GO nanocomposite filled with 1.88% GO are shown. The SEM image in the left panel reveals a good homogeneous dispersion of GO into the PVDF matrix. It is possible to observe GO aggregates ranging from very small (smaller than 30 nm) to larger ones (~300 nm). This kind of dispersion has been reported in other GO-based polymeric nanocomposites, revealing homogeneous dispersion along their cross section.[36] We think that it is the strong interactions between oxygen-containing groups, especially carbonyl groups (C═O) in GO surface and fluorine group in PVDF, that lead to the homogeneous dispersion of GO in the PVDF matrix.

The dispersion state of the four graphitic fillers are quite different. The pyrolytic graphite is dispersed in the space between spherulites. The NTCs are linked to the surface of spherulites. Both PG and MWCNTs seem to be chemical bonded to the spherulite surfaces. The aggregates of soot particles are mainly deposited in the holes (empty spaces) along the PVDF film and seem to be not bonded to the polymer chains. The nanocomposites made with these three fillers present porosity. The PVDF/GO with 1.88 wt % GO shows no porosity, which could indicate stronger interaction with the PVDF matrix.

The collected FTIR spectra for pure PVDF and PVDF-based nanocomposites filled with 1.88 wt % graphitic materials (GO, MWCNT, PG, and soot) are displayed in Figure 7a for wavenumbers ranging from 300 to 900 cm^{-1} and in Figure 7b for wavenumbers ranging from 900 to 3600 cm^{-1}. The absorption bands present in the wavenumbers range in Figure 7a are very important because they allow us to check the crystallographic phase of the PVDF nanocomposites. There are five possible distinct PVDF crystalline phases known as α, β, γ, δ, and ε phase; the β-ferroelectric pahse being the one with many technological applications, as for instance in sensors and transducers.[22] A compilation of the infrared vibrational modes related to the spectra in Figure 7 is shown in Table 1, for α, β, and γ crystalline phases. In Table 1 it is seen that, although some vibrational modes are active in the three phases, there are seven vibrational modes between 552 and 813 cm^{-1} that are active in the α and/or γ phases but are not active in the β-PVDF. Most of these vibrational modes are bending (δ-mode) or rocking (r-mode) of CF_2 and CH_2 molecules. Back to Figure 7, we see that in all spectra, including that for pure PVDF, these absorbance peaks are not present in this spectral range. This result means that all nanocomposite samples are in the β-ferroelectric phase of PVDF. In fact, the addition of nanofillers to PVDF is often performed aiming at the nucleation of the electroactive β-phase.[37,38] However, the film samples produced by casting below 80 °C show high degree of porosity and are

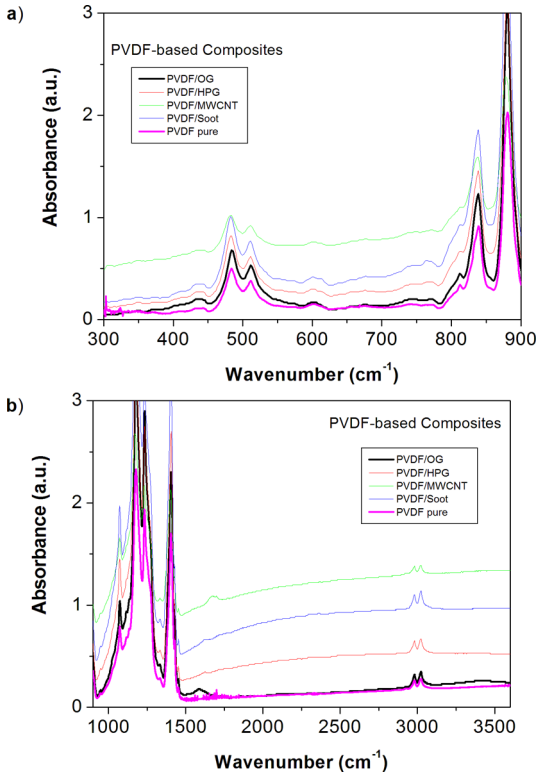

Figure 7. FTIR spectra spectra for pure PVDF and PVDF-based nanocomposites filled with 1.88 wt % graphitic materials (GO, MWCNT, PG, and soot) for wavenumbers ranging from (a) 300 to 900 cm^{-1} and (b) 900 to 3600 cm^{-1}.

Table 1. Infrared Absorption Modes for Crystalline Phases α, γ, and β of PVDF for Wavenumbers Ranging from 287 to 874 cm^{-1}[a]

α-phase		γ-phase		β-phase	
874	ν_a (CC) + υ_s (CF_2)	880	ν_a (CC) + υ_s (CF_2)	880	ν_a (CC) + υ_s (CF_2)
855	r (CH_2)	838	r (CH_2)	840	r (CH_2) - υ_s (CF_2)
		813	r (CH_2)		
796	r (CH_2)	796	r (CH_2)		
765	δ (CF_2) + δ (CCC)	776	δ (CF_2)		
		723	δ (CF_2)		
		688	δ (CF_2)		
615	δ (CF_2) + δ' (CCC)	656	δ (CF_2)		
		552	δ (CF_2)		
532	δ (CF_2)	511	δ (CF_2)		
490	δ (CF_2) + w (CF_2)	482	δ (CF_2) + w (CF_2)	508	δ (CF_2)
410	r (CF_2)			490	
		430	r (CF_2)	470	w (CF_2)
		400	r (CF_2)	445	r (CF_2) + r (CH_2)
355	t (CF_2) + r (CF_2)	348	t (CF_2) + r (CF_2)		
287	t (CF_2) + w (CF_2)	300	t (CF_2) + w (CF_2)		

[a]The symbols ν_a and ν_s represent antisymmetric and symmetric stretching modes, respectively. δ, r, w, and t represent bending, rocking, wagging, and twisting modes, respectively.

DOI: 10.1021/acs.iecr.7b02711
Ind. Eng. Chem. Res. 2017, 56, 11782−11790

not suitable for technological applications. We note that, as shown in Figures 5 and 6, among all micrographs of PVDF filled with graphitic materials, the PVDF/GO is the only one that has no apparent porosity.

The DSC thermograms of pure PVDF and PVDF-based nanocomposites filled with 1.88 wt % graphitic materials (GO, MWCNT, PG, and soot) are displayed in Figure 8 for the second thermal run (two complete cycles were made for each sample, between 25 and 200 °C, at 10 °C/min heating and cooling rates). Note that the thermograms of the pure ferroelectric copolymer show one anomaly on heating corresponding to the melting of crystallites. The anomaly on cooling corresponds to the crystallites recrystallization. The temperature of crystallization (T_M) and the corresponding melting latent heat (L_M) are displayed in Table 2. The addition of graphitic materials on the PVDF polymeric matrix leads to a decrease in both T_M and L_M. Taking into account that L_M is proportional to the crystalline volume fraction, we see that this addition accounts for a decrease of the degree of order in the crystalline cells and a reduction in the crystallite sizes. The data in Table 2 reveal that filling PVDF with graphene oxide has practically no effect on the crystallization temperature (160.0 °C against 159.3 °C). Also, GO is the one among the graphitic materials that provokes the lower decrease in L_M and, consequently, in the crystalline fraction.

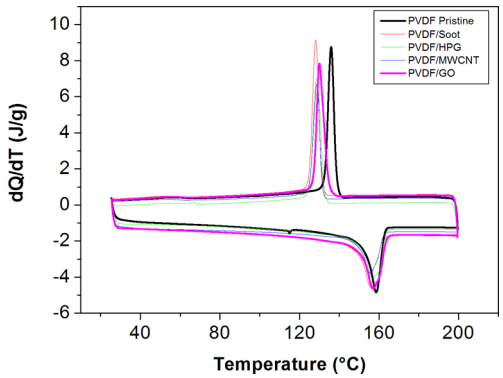

Figure 8. DSC thermograms of pure PVDF and PVDF-based nanocomposites filled with 1.88 wt % graphitic materials (GO, MWCNT, PG, and soot) for the second thermal run. Two complete cycles were made for each sample, between 25 and 200 °C, at 10 °C/min heatin and cooling rates.

Table 2. Temperature of Crystallization (T_M) and Melting Latent Heat (L_M) Taken from Figure 8 for Pure PVDF and PVDF-Based Nanocomposites Filled with 1.88 wt % Graphitic Materials (GO, MWCNT, PG, and Soot)

	PVDF	PVDF/GO	PVDF/PG	PVDF/MWCNT	PVDF/soot
melting latent heat (J/g)	44.1	39.57	30.28	28.8	34.4
melting temperature (°C)	160.0	159.3	150.8	155.7	155.9

Once it is reported that one monolayer of graphene absorbs ≈2.3% of incident white (visible) light, we may now check if the addition of a small amount of graphene oxide into the PVDF matrix changes its transparence in the ultraviolet−visible spectral region by collecting the optical absorbance spectra of the nanocomposites. These spectra are shown in Figure 9. We see that the addition of pyrolytic graphite and soot makes practically no changes in the absorbance spectrum of PVDF above 400 nm. However, from 240 to 400 nm, the nanocomposites decrease the original optical absorbance. Interestingly, the addition of GO increases the absorbance in the 400−700 nm, which is the visible region, in agreement with the data reported by Nair et al.[6] The wide absorption peak at 250 nm is a sum of the graphene oxide absorption at 230 nm and the doublet of conjugated C═C bonds (223 nm) and triplet (274 nm) of PVDF. The spectrum of PVDF/MWCNT is very similar to the GO spectrum. MWCNT also has an absorption peak at 230 nm.

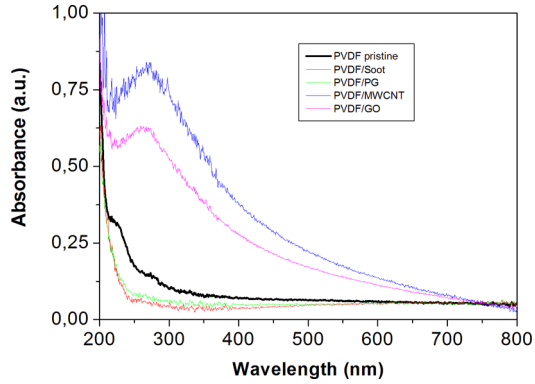

Figure 9. UV−vis absorbance spectra of pure PVDF and PVDF-based nanocomposites filled with 1.88 wt % graphitic materials (GO, MWCNT, PG, and soot) for wavelengths ranging from 200 to 800 nm.

Finally, we discuss the estimation of radio-induced damages in PVDF/GO nanocomposites, filled with 1.88 wt % GO, provoked by exposure to high doses of ionizing radiation beams. This issue is directly linked to the economic practical aspects involved in the life cycle of safety instruments and radiopaque fabrics used for protection against X-ray radiation. The defects induced by ionizing radiation in macromolecules are well-known to be cumulative for successive radiation exposures. In this context, PVDF homopolymer is one of the most radiation resistant polymers commercially available. Its radiation stability is reported to be maintained for γ doses as high as 1000 kGy.[39] In the case of PVDF membranes, its integrity is reported to be unaltered until 50 MRad (500 kGy).[40]

In order to obtain preliminary information about the radio-resistance of PVDF/GO nanocomposites, we have irradiated pure PVDF and PVDF/GO samples with increased γ doses until 1000 kGy and evaluated the associated radio-damage by FTIR spectrometry. The FTIR spectra for samples irradiated with 1000 kGy are displayed in Figure 10 for wavenumbers ranging from 1500 to 1950 cm^{-1}. The wide absorption peak observed at 1730 cm^{-1} in the irradiated PVDF spectrum is attributed to the sum of the radio-induced peaks at 1715 cm^{-1} (C═C stretching), 1730 cm^{-1} (C═O dimer stretch), and 1754 cm^{-1} (C═C stretching), and the peak at 1853 cm^{-1} is attributed to stretch of C═O bonds.[41] The wide peak observed in the PVDF/GO spectrum is attributed to graphene oxide. We remark that the radio-induced peaks present in the irradiated PVDF spectrum are not present in the PVDF/GO spectrum. This result means that the GO structures are resistant to the radiation dose applied (1000 kGy) and, more importantly, their presence in the polymeric matrix improves the radiation-resistance of PVDF by preventing radio-oxidation and the

DOI: 10.1021/acs.iecr.7b02711
Ind. Eng. Chem. Res. 2017, 56, 11782−11790

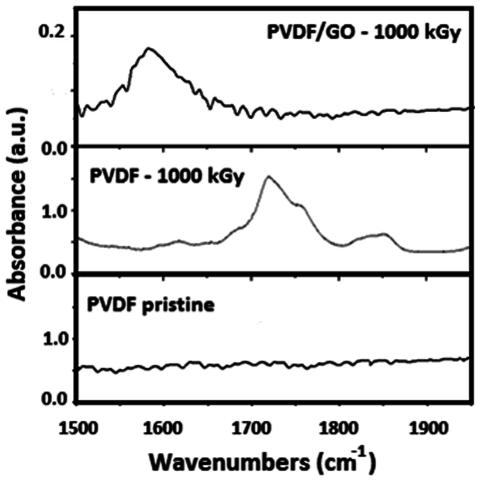

Figure 10. FTIR spectra of γ-irradiated (1000 kGy) samples of PVDF/GO nanocomposite (upper) and pure PVDF (bottom).

formation of C═C bonds. We believe that this phenomenon is a preliminary indication that the PVDF/GO nanocomposite maintains the original radiation integrity of PVDF homopolymer until 1000 kGy or even more. However, we think that a complete structural integrity test should be performed to confirm this conclusion.

4. CONCLUSIONS

We have demonstrated the increased X-ray attenuation efficiency of graphene-based nanocomposites. For 6.9 keV photons, the mass attenuation coefficient value measured for PVDF/GO nanocomposite filled with 1.88 wt % GO was found to be four times higher than that encountered for nanocomposites made of PVDF filled with 1.88 wt % functionalized graphene oxides, pyrolytic graphite, multiwalled carbon nanotubes, and amorphous carbon (soot). The mechanisms of these observations are not clear and need further elucidation. The mass attenuation coefficients were measured for X-ray photons with 6.9, 8.1, 17.5, and 22.1 keV, respectively. The enhanced attenuation appears in the region where photoelectric absorption starts to predominate against coherent and incoherent scattering, toward lower energies. FTIR data reveal that all nanocomposites studied are in the ferroelectric β-phase of PVDF. After irradiation with 1.0 MGy of γ dose, it was demonstrated that the addition of graphene oxide to the PVDF matrix improves its radiation resistance by preventing radio-oxidation and the formation of C═C bonds. Lightweight, very thin, and highly efficient PVDF/GO radiopaque films can be now manufactured, aiming to minimize patient skin injuries in high-dose interventional radiology procedures.

AUTHOR INFORMATION

Corresponding Author

*E-mail: farialo@cdtn.br. Tel.: 55 31 30693128.

ORCID

Luiz O. Faria: 0000-0003-2523-8640

Notes

The authors declare no competing financial interest.

ACKNOWLEDGMENTS

The authors acknowledge the financial support from the Brazilian government agencies Conselho Nacional de Pesquisa e Desenvolvimento (CNPq) and Fundação de Amparo a Pesquisa do Estado de Minas gerais (FAPEMIG).

REFERENCES

(1) Novoselov, K. S.; Geim, A. K.; Morozov, S. V.; Jiang, D.; Zhang, Y.; Dubonos, S. V.; Grigorieva, I. V.; Firsov, A. A. Electric Field Effect in Atomically Thin Carbon Films. *Science* **2004**, *306*, 666.

(2) Cheng, Q. F.; Wang, J. P.; Wen, J. J.; Liu, C. H.; Jiang, K. L.; Li, Q. Q.; Fan, S. S. Carbon nanotube/epoxy composites fabricated by resin transfer molding. *Carbon* **2010**, *48*, 260.

(3) Fang, M.; Wang, K.; Lu, H.; Yang, Y.; Nutt, S. Single-layer graphene nanosheets with controlled grafting of polymer chains. *J. Mater. Chem.* **2010**, *20*, 1982.

(4) Chen, J.; Yao, B.; Li, C.; Shi, G. An improved Hummers method for eco-friendly synthesis of graphene oxide. *Carbon* **2013**, *64*, 225.

(5) Li, Z.; Chen, L.; Meng, S.; Guo, L.; Huang, J.; Liu, Y.; Wang, W.; Chen, X. Field and temperature dependence of intrinsic diamagnetism in graphene: Theory and experiment. *Phys. Rev. B: Condens. Matter Mater. Phys.* **2015**, *91* (9), 094429.

(6) Nair, R. R.; Blake, P.; Grigorenko, A. N.; Novoselov, K. S.; Booth, T. J.; Stauber, T.; Peres, N. M. R.; Geim, A. K. Fine Structure Constant Defines Visual Transparency of Graphene. *Science* **2008**, *320*, 1308.

(7) Rubrice, K.; Castel, X.; Himdi, M.; Parneix, P. Dielectric Characteristics and Microwave Absorption of Graphene Composite Materials. *Materials* **2016**, *9*, 825.

(8) Kuilla, T.; Bhadra, S.; Yao, D.; Kim, N. H.; Bose, S.; Lee, J. H. Recent advances in graphene based polymer composites. *Prog. Polym. Sci.* **2010**, *35*, 1350.

(9) Miller, D. L.; Balter, S.; Cole, E. P.; Lu, T. H.; Schueler, B. A.; Geisinger, M.; Berenstein, A.; Albert, R.; Georgia, J. G.; Noonan, P. T.; Cardella, J. F.; George, J. S.; Russell, E. J.; Malisch, T. W.; Vogelzang, R. L.; Miller, G. L., III; Anderson, J. Radiation Doses in Interventional Radiology Procedures: The RAD-IR Study Part I: Overall Measures of Dose. *J. Vasc. Interv. Radiology* **2003**, *14*, 711.

(10) Brambilla, M.; Marano, G.; Dominietto, M.; Cotroneo, A. R.; Carriero, A. Patient radiation doses and references levels in interventional radiology. *Radiol. Med.* **2004**, *107* (4), 408.

(11) Fujimori, T.; Tsuruoka, S.; Fugetsu, B.; Maruyama, S.; Tanioka, A.; Terrones, M.; Dresselhaus, M. S.; Endo, M.; Kaneko, K. Enhanced X − Ray Shielding Effects of Carbon nanotubes. *Mater. Express* **2011**, *1* (4), 273.

(12) Fujikawa, T.; Arai, H. Theory of phonon effects on photoemission spectra. *J. Electron Spectrosc. Relat. Phenom.* **2009**, *174*, 85.

(13) Fujikawa, T. New developments in theory of X-ray photoemission from solids. *J. Electron Spectrosc. Relat. Phenom.* **2009**, *173*, 51.

(14) Sawada, K.; Murakami, S.; Nagaosa, N. Dynamical diffraction theory for wave packet propagation in deformed crystals. *Phys. Rev. Lett.* **2006**, *96*, 154802.

(15) Zhang, B.; Wang, Y.; Zhai, G. Biomedial aplications of the graphene-based materials. *Mater. Sci. Eng., C* **2016**, *61*, 953.

(16) Armstrong, G. An introduction to polymer nanocomposites. *Eur. J. Phys.* **2015**, *36*, 063001.

(17) Hussain, F.; Hojjati, M.; Okamoto, M.; Gorga, R. E. Review article: Polymer-matrix nanocomposites, processing, manufacturing, and application: An overview. *J. Compos. Mater.* **2006**, *40* (17), 1511.

(18) Camargo, P. H. C.; Satyanarayana, K. G.; Wypych, F. Nanocomposites: Synthesis, structure, properties and new application opportunities. *Mater. Res.* **2009**, *12* (1), 1.

(19) Nambiar, S.; Yeow, J. T. W. Polymer-Composite Materials for Radiation Protection. *ACS Appl. Mater. Interfaces* **2012**, *4*, 5717.

(20) Fontainha, C. C. P.; Baptista-Neto, A. T.; Santos, A. P.; Faria, L. O. P(VDF-TrFE)/ZrO2 Polymer-Composites for X-ray Shielding. *Mater. Res.* **2016**, *19*, 426.

(21) Li, Z.; Chen, S.; Nambiar, S.; Sun, Y.; Zhang, M.; Zheng, W.; Yeow, J. T. W. PMMA/MWCNT nanocomposite for proton radiation shielding applications. *Nanotechnology* **2016**, *27*, 234001.

(22) Lovinger, A. J. Ferroelectric Polymers. *Science* **1983**, *220* (4602), 1115.

DOI: 10.1021/acs.iecr.7b02711
Ind. Eng. Chem. Res. 2017, 56, 11782−11790

(23) Prateek; Thakur, V. K.; Gupta, R. K. Recent Progress on Ferroelectric Polymer-Based Nanocomposites for High Energy Density Capacitors: Synthesis, Dielectric Properties, and Future Aspects. *Chem. Rev.* **2016**, *116* (7), 4260.
(24) Al-Saygh, A.; Ponnamma, D.; AlMaadeed, M. A.; Vijayan, P.; Karim, A.; Hassan, M. K. Flexible Pressure Sensor Based on PVDF Nanocomposites Containing Reduced Graphene Oxide-Titania Hybrid Nanolayers. *Polymers* **2017**, *9*, 33.
(25) Tsonos, C.; Pandis, C.; Soin, N.; Sakellari, D.; Myrovali, E.; Kripotou, S.; Kanapitsas, A.; Siores, E. Multifunctional nanocomposites of poly(vinylidene fluoride) reinforced by carbon nanotubes and magnetite nanoparticles. *eXPRESS Polym. Lett.* **2015**, *9* (12), 1104.
(26) Ataur Rahman, Md.; Chung, G. Synthesis of PVDF-graphene nanocomposites and their properties. *J. Alloys Compd.* **2013**, *581*, 724.
(27) Ataur Rahman, Md.; Lee, B.; Phan, D.; Chung, G. Fabrication and characterization of highly efficient flexible energy harvesters using PVDF−graphene nanocomposites. *Smart Mater. Struct.* **2013**, *22* (8), 085017.
(28) Jang, J. W.; Min, B. G.; Yeum, J. H.; Jeong, Y. G. Structures and physical properties of graphene/PVDF nanocomposite films prepared by solution-mixing and melt-compression. *Fibers Polym.* **2013**, *14*, 1332.
(29) Marcano, D. C.; Kosynkin, D. V.; Berlin, J. M.; Sinitskii, A.; Sun, Z.; Slesarev, A.; Alemany, L. B.; Lu, W.; Tour, J. M. Improved synthesis of graphene oxide. *ACS Nano* **2010**, *4* (8), 4806.
(30) Hubbel, J. H.; Seltzer, M. Table of X-ray mass attenuation coefficients from 1 keV to 20 MeV for elements Z = 1 to 92 and 48 additional substances of dosimetric interest. NIST Standard Database 126; National Institute of Standards and Technology: Gaithersburg, MD, 2004.
(31) Bludov, Y. V.; Peres, N. M. R.; Vasilevskiy, M. I. Unusual reflection of electromagnetic radiation from a stack of graphene layers at oblique incidence. *J. Opt.* **2013**, *15*, 114004.
(32) Yoon, D.; Son, Y.-W.; Cheong, H. Negative Thermal Expansion Coefficient of Graphene Measured by Raman Spectroscopy. *Nano Lett.* **2011**, *11* (8), 3227.
(33) Ma, W.; Zhang, J.; Wang, X. Effect of Initial Polymer Concentration on the Crystallization of Poly (Vinylidene Fluoride)/Poly (Methyl Methacrylate) Blend from Solution Casting. *J. Macromol. Sci., Part B: Phys.* **2008**, *47*, 139.
(34) Gregorio, R., Jr.; Marcelo, C. Effect of crystallization temperature on the crystalline phase content and morphology of poly(vinylidene fluoride). *J. Polym. Sci., Part B: Polym. Phys.* **1994**, *32*, 859.
(35) Gelfandbein, V.; Perlman, M. M. Substrate effects on crystallization of polyvinylidene fluoride from solution. *J. Mater. Sci.* **1983**, *18*, 3183.
(36) Gahlot, S.; Kulshrestha, V.; Agarwal, G.; Jha, P. K. Synthesis and Characterization of PVA/GO Nanocomposite Films. *Macromol. Symp.* **2015**, *357*, 173.
(37) Martins, P.; Caparros, C.; Goncalves, R.; Martins, P. M.; Benelmekki, M.; Botelho, G.; Lanceros-Mendez, S. Role of Nanoparticle Surface Charge on the Nucleation of the Electroactive β-Poly(vinylidene fluoride) Nanocomposites for Sensor and Actuator Applications. *J. Phys. Chem. C* **2012**, *116*, 15790.
(38) Layek, R. K.; Samanta, S.; Chatterjee, D. P.; Nandi, A. K. Physical and mechanical properties of poly(methyl methacrylate)-functionalized graphene/poly(vinylidine fluoride) nanocomposites: Piezoelectric β polymorph formation. *Polymer* **2010**, *51*, 5846.
(39) Nordion Inc. Gamma Compatible Materials. Reference Guide, Printed in Canada. PCCS 121D, 2011.
(40) Mohapatra, P. K.; Raut, D. R.; Shah, J. G.; Bhardwaj, Y. K. Studies on the Radiation Stability of Several Polymeric Flat Sheets used for Actinide Ion Separation from Radioactive Feeds. *J. Membr. Sci. Technol.* **2016**, *6*, 157.
(41) Boullier, I.; Esnouf, S.; Le Moël, A. Radiooxidation of fluoropolymers: identification of oxidation products. *J. Polym. Sci., Part B: Polym. Phys.* **2003**, *41*, 1509.

DOI: 10.1021/acs.iecr.7b02711
Ind. Eng. Chem. Res. 2017, 56, 11782−11790